

## ***Supporting Information***

### **Construction and multifunctional applications of visible-light-excited multicolor long afterglow carbon dots/boron oxide composites**

*Wei He, Xiangying Sun\*, Xuegong Cao*

*College of Materials Science and Engineering, Huaqiao University, Key Laboratory of Molecular Designing and Green Conversions (Fujian University), NO. 668 Jimei Avenue, Jimei District, Xiamen 361021, China*

***To whom correspondence should be addressed:***

*\*(Xiangying Sun) E-mail: sunxy@hqu.edu.cn*

Number of pages: 27

Number of Figures: 28 (Figure S1, S2, S3, S4, S5, S6, S7, S8, S9, S10, S11, S12, S13, S14, S15, S16, S17, S18, S19, S20, S21, S22, S23, S24, S25, S26, S27, and S28)

Number of Tables: 2 (Table S1 and S2)

## Experimental section

### Materials and instruments

**Materials.** Safranin T, rhodamine 6G, NaOH, boric acid, sulfuric acid, ethanol, polyvinyl alcohol, citric acid, urea, starch, and NaCl were purchased from Sinopharm Chemical Reagent Co., Ltd (Shanghai, China). Fluorescein isothiocyanate isomer, rhodamine B, m-Phenylenediamine, tetraethoxysilane, and TiO<sub>2</sub> were purchased from Aladdin (Shanghai, China). Fuchsin basic were supplied by Macklin(Shanghai, China). Ultrapure water was prepared by a Milli-Q water purification system (USA).

**Instruments.** All fluorescence spectra were recorded by a HITACHI F-7000 fluorescence spectrometer (Hitachi, Japan). Absorption spectra were measured with a UV-2600 UV-Vis spectrophotometer (Shimadzu, Japan) and a Cary 5000 UV-Vis-NIR spectrophotometer (Agilent, USA). Morphology of samples was recorded by transmission electron microscope (TEM, FEI Talos F200s, America). Fluorescence and afterglow lifetime decay curves were obtained by employing a FS5 fluorescence spectrometer (Edinburgh Instruments, UK). Fluorescence quantum yield and afterglow quantum yield were measured with a FLS920 fluorescence spectrometer (Edinburgh Instruments, UK) and a FLS980 fluorescence spectrometer (Edinburgh Instruments, UK), respectively. X-ray diffraction (XRD) was performed using a Rigaku SmartLab. The X-ray photoelectron spectra (XPS) were recorded on a Quantum-2000 electron spectrometer (Physical electronics Co., Ltd). The Fourier transform infrared (FTIR) spectra were taken by a FTIR-4800s spectrophotometer

(Shimadzu Co., Ltd).

### **Synthesis of CDs**

**Synthesis of CDs-II.** The CDs-II were prepared according to the reported method<sup>1</sup>. 100 mg rhodamine B (RHB) was dissolved in 20 mL 0.5 M NaOH solution, and the solution was sonicate for 10 min to completely dissolve RHB. Then, the mixed solution was transferred into a 50 mL polytetrafluoroethylene lined autoclaves and heated at 200 °C for 5 h. After the solution was naturally cooled to room temperature, it was stored in a refrigerator at 4 °C.

**Synthesis of CDs-III.** 100 mg fluorescein isothiocyanate isomer (FITC) was dissolved in 20 mL 0.5 M NaOH solution, and sonicate for 10 min to completely dissolve FITC. Then the mixed solution was transferred into a 50 mL polytetrafluoroethylene lined autoclaves and heated at 200 °C for 5 h. After the solution was naturally cooled to room temperature, it was stored in a refrigerator at 4 °C.

**Synthesis of CDs-IV.** 100 mg fuchsin basic (FB) was dissolved in 20 mL 0.5 M NaOH solution, and sonicate for 10 min to completely dissolve FB. Then the mixed solution was transferred into a 50 mL polytetrafluoroethylene lined autoclaves and heated at 200 °C for 5 h. After the solution was naturally cooled to room temperature, it was stored in a refrigerator at 4 °C..

**Synthesis of CDs-V.** 100 mg rhodamine 6G (R6G) was dissolved in 20 mL 0.5 M NaOH solution, and sonicate for 10 min to completely dissolve R6G. Then the mixed solution was transferred into a 50 mL polytetrafluoroethylene lined autoclaves

and heated at 200 °C for 5 h. After the solution was naturally cooled to room temperature, it was stored in a refrigerator at 4 °C.

**Synthesis of CDs-VI.** The CDs-VI were prepared according to the reported method<sup>2</sup>. 200 mg m-Phenylenediamine was dissolved in 20 mL ethanol, and add 1 mL H<sub>2</sub>SO<sub>4</sub>. Then the mixed solution was transferred into a 50 mL polytetrafluoroethylene lined autoclaves and heated at 200 °C for 10 h. After being naturally cooled to room temperature, remove the lower layer solution and keep the upper layer solution by extraction, then stored in a refrigerator at 4 °C.

#### **Synthesis of multicolor CDs/B<sub>2</sub>O<sub>3</sub> composites**

Specifically, 2 g boric acid was diluted with 40 mL DI water and mixed with 2 mL CDs(CDs- II , CDs-III, CDs-IV, CDs- V , and CDs-VI) in a beaker by ultrasonic for 10 min. Then the beaker was covered with foil to prevent the water from evaporating too fast. Afterwards, the beaker was put in an oven at 180 °C for 5 h and cooled down to room temperature naturally, the amorphous glassy state composites were obtained. The final products(CDs- II/B<sub>2</sub>O<sub>3</sub>, CDs-III/B<sub>2</sub>O<sub>3</sub>, CDs-IV/B<sub>2</sub>O<sub>3</sub>, CDs- V/B<sub>2</sub>O<sub>3</sub>, and CDs-VI/B<sub>2</sub>O<sub>3</sub>) were ground into powder.

#### **Synthesis of CDs powder with only fluorescence**

The synthesis of CDs powder with only fluorescence refers to the previous work of our group<sup>3</sup>. 1.5 g citric acid and 8.1 mg of ST that had the molar ratio is 1000:3 were dissolved in 10 mL water, followed by stirring for a period of two minutes for the formation of an integrated mixture solution. Subsequent to that, the mixture was transferred into an autoclave inner vessel, together with placing in an oven at a

temperature of 170 °C for a period of six hours. The final CDs solution was freeze-dried to powder at -40 °C under vacuum.

### **Synthesis of different CDs-I-based composites**

**CDs-I/urea.** 2 mL CDs-I aqueous solution were mixed with urea (6 g) to obtain CDs-I/urea solutions in beakers by shaking for 10 min to completely dissolve the urea. Then the beakers were put into oven at 155 °C for 6 h and cooled down to room temperature naturally. The final products (CDs-I/urea) were ground into powder.

**CDs-I/NaCl.** 2 mL CDs-I aqueous solution were added to saturate NaCl solution and stirred for 10 min, then the mixed solution was added to the bottom of methanol solution, after standing for 48 h, CDs-I/NaCl was precipitated, and the product was ground into powder.

**CDs-I/PVA.** 200  $\mu$ L CDs-I aqueous solution were firstly diluted with 300  $\mu$ L DI water, and then mixed with 1.5 mL of polyvinyl alcohol(PVA) solution (1.0 g in 15 mL water). Then dry the sample in a 60 °C oven for 6 h to obtain CDs-I/PVA film.

**CDs-I/SiO<sub>2</sub>.** 2 mL CDs-I aqueous solution and 1 mL tetraethoxysilane were dispersed in 25 mL deionized water to form aqueous solution. Then, the above solution was stirring at room temperature for 5 h. The transparent solution was filtered through 0.22  $\mu$ m membrane for three times. Finally, the final CDs-I/SiO<sub>2</sub> solution was freeze-dried to a powder at -40 °C.

**CDs-I/TiO<sub>2</sub>.** 2 mL CDs-I aqueous solution and 0.4 g TiO<sub>2</sub> were dispersed in a mixed solution of 26 mL of deionized water and ethanol( $V_{\text{water}}:V_{\text{ethanol}}=3:10$ ). Then the mixed solution was transferred into a 50 mL polytetrafluoroethylene lined

autoclaves and heated at 140 °C for 4 h. The product was centrifuged for 10 minutes to remove the supernatant, and then the solid was placed in a 60°C oven to dry for 24 h to obtain CDs-I/TiO<sub>2</sub> powder.

**CDs-I/starch.** 2 mL CDs-I aqueous solution and 2 g starch were dispersed in 40 mL DI water to form aqueous solution. After stirring the mixed solution for 12 h at room temperature, centrifuge for 10 minutes, remove the supernatant, and place the solid in a 60 °C oven to dry for 24 h to obtain CDs-I/starch powder.

### **Measurement of fluorescence quantum yield (QY) of CDs solution**

The QY measurement was calculated according to the following equation:

$$\varphi_S = \varphi_R \frac{Grad_S \eta_S^2}{Grad_R \eta_R^2} \quad (1)$$

where S and R refer to standard group and test group (CDs solution), respectively;  $\varphi$  represents fluorescence quantum yield; A is the absorbance,  $G_{rad}$  means the gradient from the plot of integrated fluorescence intensity against absorbance; and  $\eta$  is the refractive index of the solvent (1.33 for water). Fluorescence quantum yield ( $\varphi_R$ ) of quinine sulfate (0.1 M H<sub>2</sub>SO<sub>4</sub>) is 0.54 under 360 nm excitation

### **Ratiometric and reversible temperature sensing based on CDs-I/B<sub>2</sub>O<sub>3</sub> composites**

As shown in Figure S19A, as the temperature increases from 20 °C to 80 °C, the phosphorescence gradually decreases until it is completely converted to TADF, which is because increasing the temperature promotes non-radiative transitions, thereby reducing phosphorescence emission and enhancing and promoting TADF emission. Similarly, the RTP is recovered and TADF gradually decreases when the temperature decreases from 80 °C to 20 °C (Figure S19B). As shown in Figure S20, the lifetime of

CDs-I/B<sub>2</sub>O<sub>3</sub> is obviously decreasing as the temperature gradually increasing and when the temperature drops from 80 °C to 20 °C, the lifetime is restored. Figure S19C plots the integrated intensity ratio of 450-545 nm (A<sub>1</sub>, TADF) to 545-650 nm (A<sub>2</sub>, RTP) versus temperature (20-80 °C and 80-20 °C), and a Gaussian fitted relationship with a good linearity was obtained, which can be described as:

$$\frac{A_1}{A_2} = 0.2038 + 0.2567T \text{ (Heating process)} \quad (1)$$

$$\frac{A_1}{A_2} = 0.1385 + 0.2649T \text{ (Cooling process)} \quad (2)$$

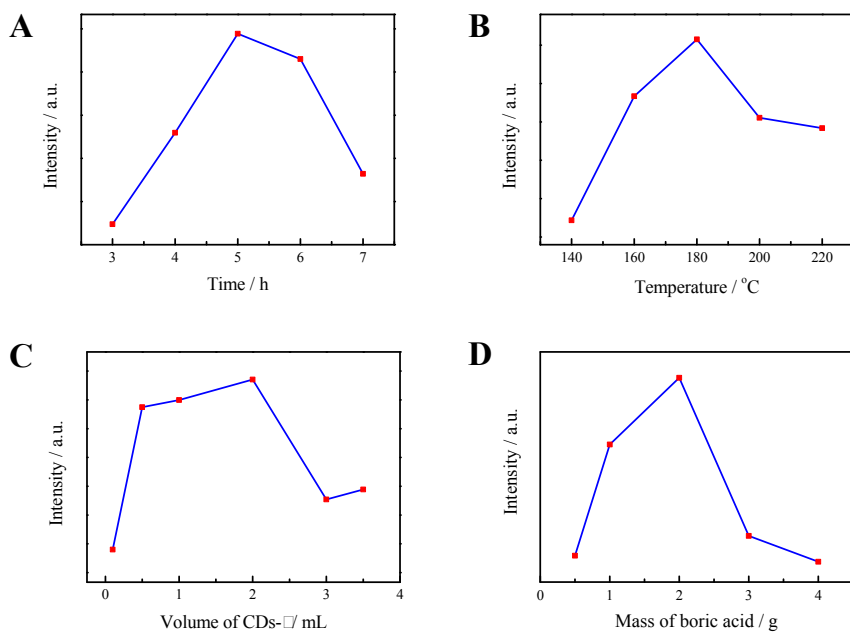
its correlation coefficient is about 0.995(Heating) and 0.990(Cooling), respectively, where T represents the temperature (°C).

A cyclic operation was put to use for the purpose of evaluating the reversibility and stability of the fluorescence severity of the CDs-I/B<sub>2</sub>O<sub>3</sub> composites. Figure S19D reveals the fact that A<sub>1</sub>/A<sub>2</sub> of the CDs-I/B<sub>2</sub>O<sub>3</sub> composites was hardly changed subsequent to the five cycles of repetition, indicating that CDs-I/B<sub>2</sub>O<sub>3</sub> composites have high stability and reversibility with temperature changes.

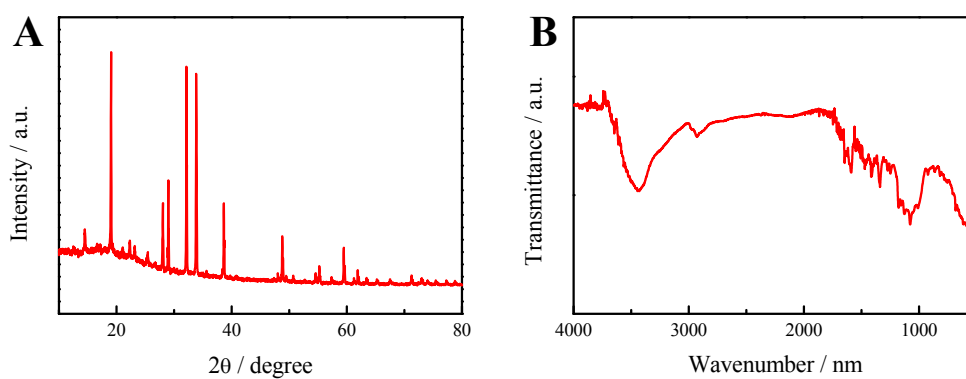
The UV-Vis absorbance spectrum of CDs-I/B<sub>2</sub>O<sub>3</sub> composites was recorded at different temperatures (Figure S23). Neither the position nor the intensity of the absorption band of CDs-I/B<sub>2</sub>O<sub>3</sub> composites changed with the temperature increment, which shows that the structure of CDs-I/B<sub>2</sub>O<sub>3</sub> composites has not changed significantly and the band gap of CDs-I/B<sub>2</sub>O<sub>3</sub> composites has little dependence on temperature. The results were consistent with those of previously reported CDs. To further evaluate the sensing mechanism, the afterglow spectra of CDs-I/B<sub>2</sub>O<sub>3</sub> composites were deconvoluted using the multi-Gaussian function. As shown in

Figure S26, the afterglow spectrum of CDs-I/B<sub>2</sub>O<sub>3</sub> composites can be easily fitted to three Gaussian functions with the temperature increment. Through the deconvolution spectrum, it is found that the three peaks of CDs-I/B<sub>2</sub>O<sub>3</sub> composites have changed significantly with the increase of temperature (Figure S27). It suggests that the temperature dependence of CDs-I/B<sub>2</sub>O<sub>3</sub> composites is similar to that of metal semiconductors and inorganic quantum dots.

## Figure



**Figure S1.** CDs- I/B<sub>2</sub>O<sub>3</sub> prepared under various (A) reaction times, (B) reaction temperatures, (C) volumes of CDs-I, and (D) mass of boric acid.



**Figure S2.** (A) XRD patterns and (B) FTIR spectra of ST.

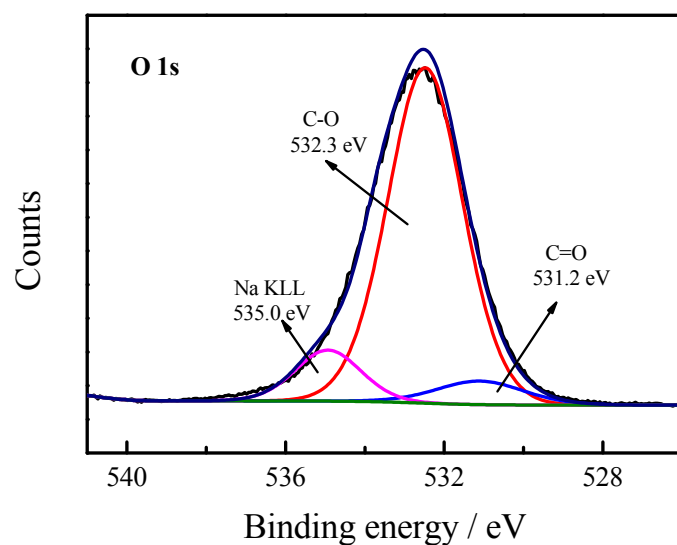


**Figure S3.** O 1s XPS of CDs-I/B<sub>2</sub>O<sub>3</sub> composites.

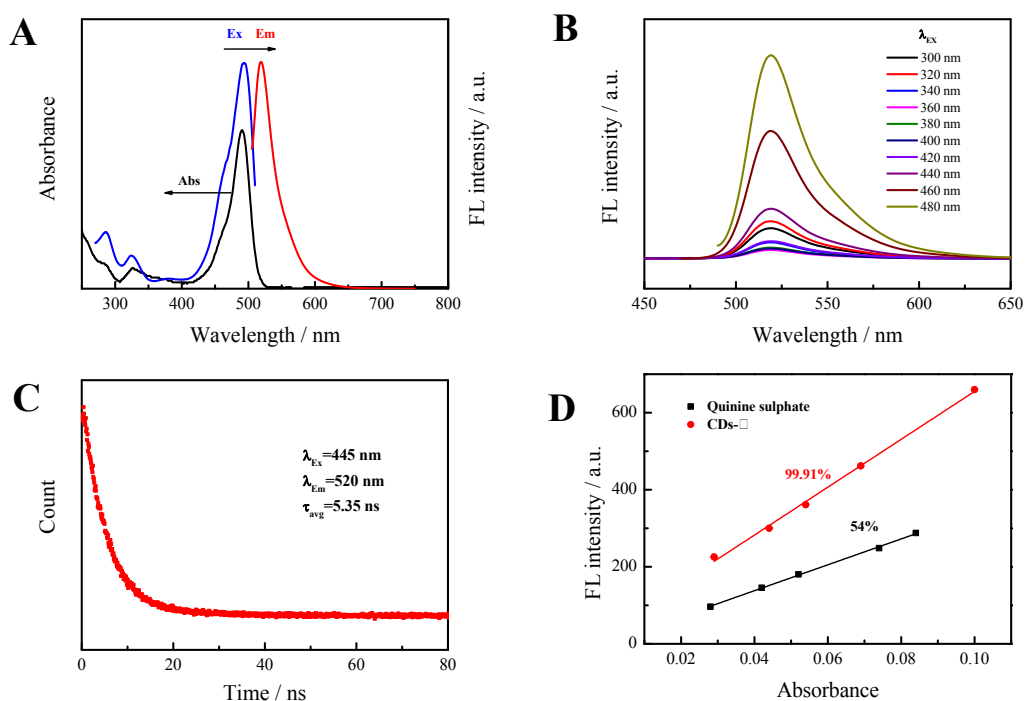


**Figure S4.** (A) UV-vis absorption, fluorescence excitation, and emission spectra of CDs-I in aqueous solution. (B) Fluorescence emission spectra of CDs-I in aqueous solution subjected to the varying excitation wavelengths that range between 300 and 500 nm. (C) Fluorescence lifetime of CDs-I in aqueous solution. (D) Linear relationship between fluorescence intensity and absorption value.

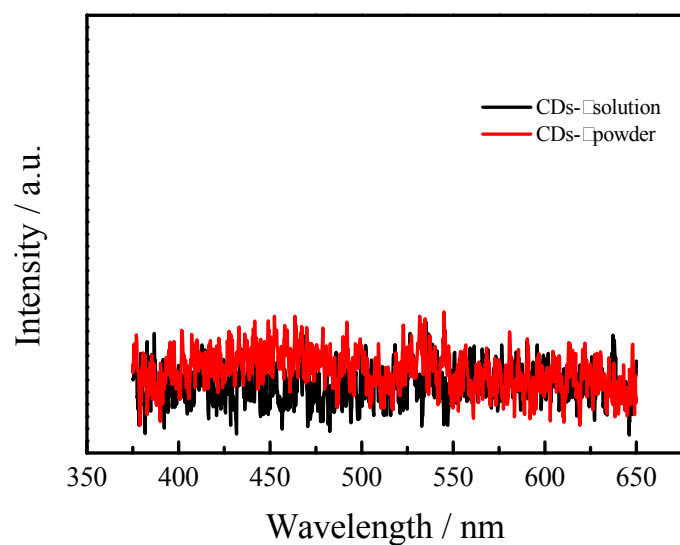


**Figure S5.** Afterglow spectra of CDs-I solution and CDs-I powder.

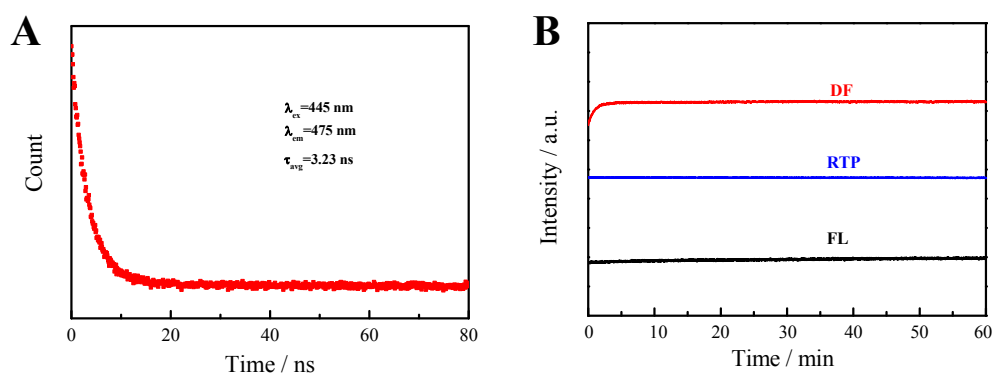


**Figure S6.** (A) Fluorescence lifetime of CDs-I/B<sub>2</sub>O<sub>3</sub> composites. (B) Fluorescence and afterglow emission intensities of CDs-I/B<sub>2</sub>O<sub>3</sub> composites during continuous excitation with a UV lamp up to 60 min.

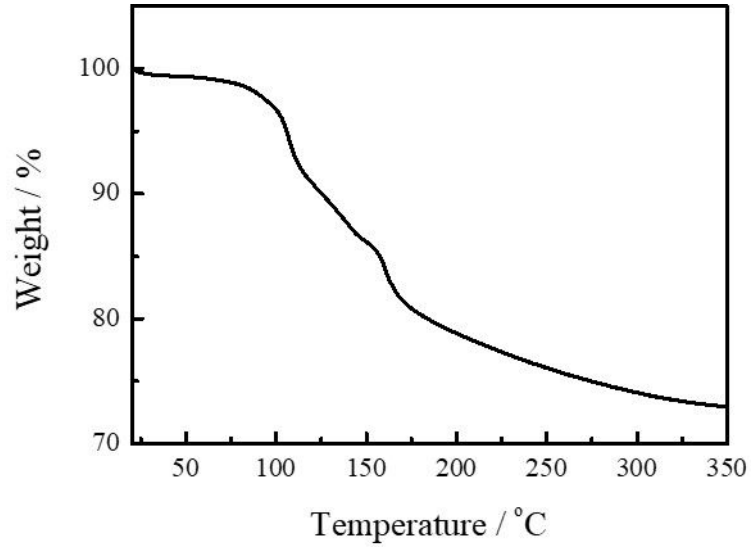


**Figure S7.** TG curve of CDs-I/ $B_2O_3$  composites.

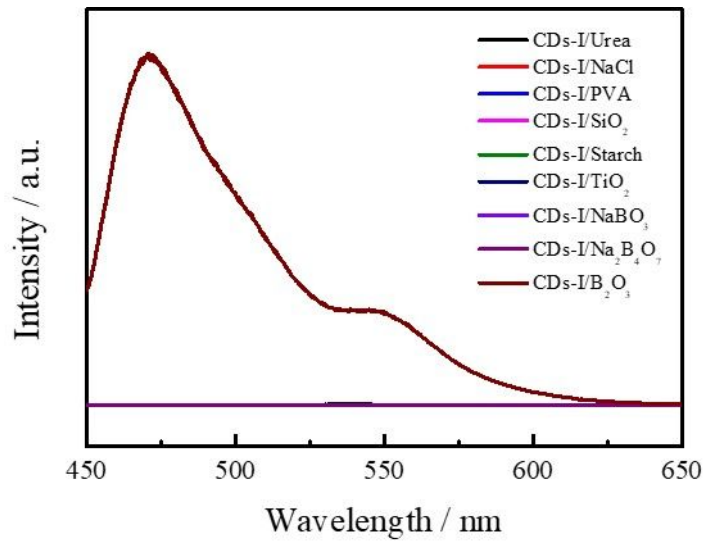


**Figure S8.** Afterglow spectra of CDs-I mixed into different matrices.

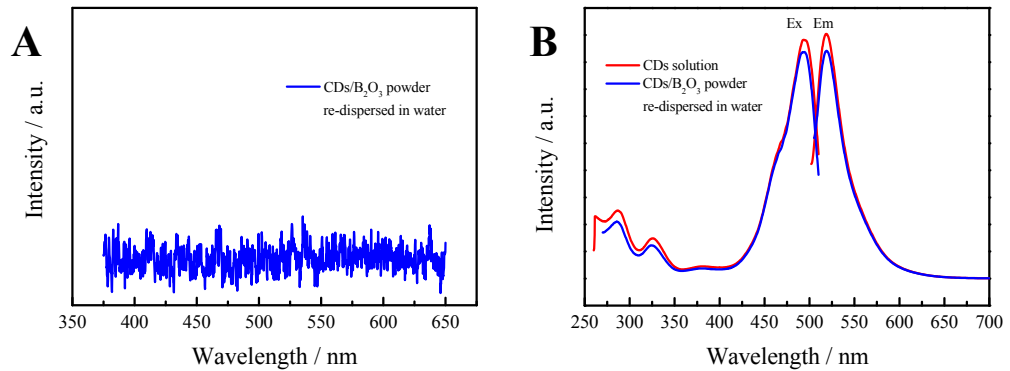


**Figure S9.** (A) Afterglow spectra of CDs-I/B<sub>2</sub>O<sub>3</sub> re-dispersed in water. (B) Fluorescence excitation and emission spectra of CDs-I solution and CDs-I/B<sub>2</sub>O<sub>3</sub> re-dispersed in water.

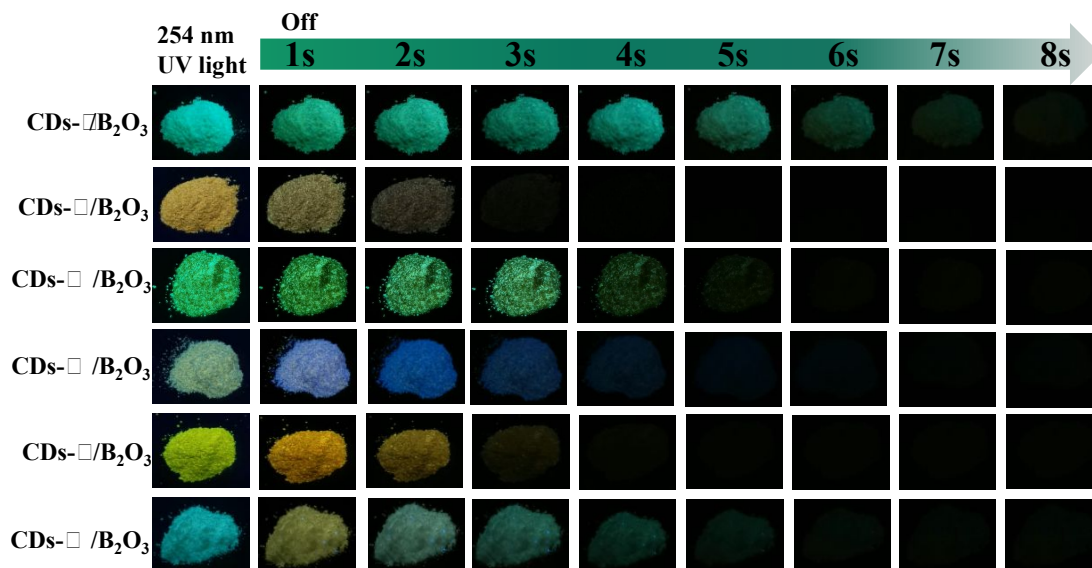


**Figure S10.** Digital photographs of different CDs/B<sub>2</sub>O<sub>3</sub> composites before and after removing 254 nm light.

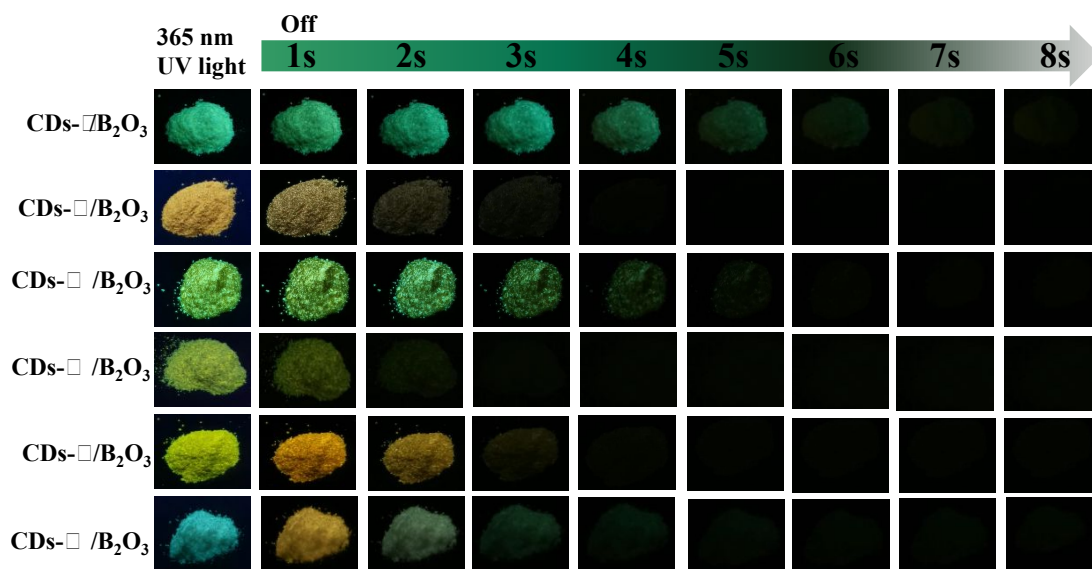


**Figure S11.** Digital photographs of different CDs/B<sub>2</sub>O<sub>3</sub> composites before and after removing 365 nm light.

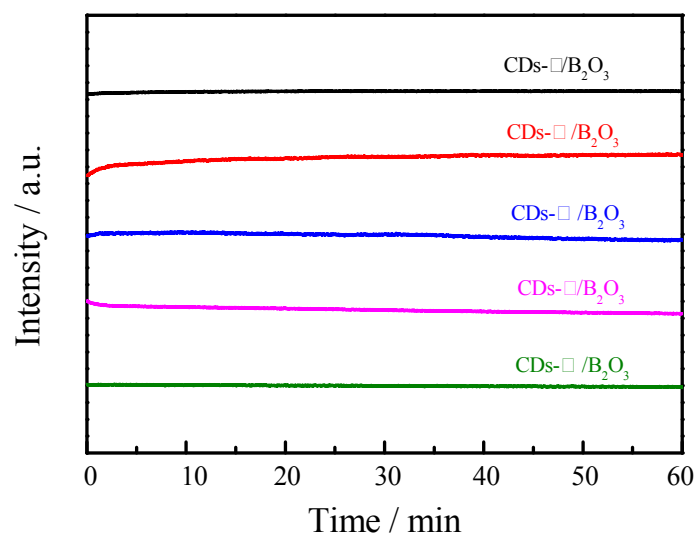


**Figure S12.** Afterglow emission intensities of CD<sub>s</sub>-II/B<sub>2</sub>O<sub>3</sub>, CD<sub>s</sub>-III/B<sub>2</sub>O<sub>3</sub>, CD<sub>s</sub>-IV/B<sub>2</sub>O<sub>3</sub>, CD<sub>s</sub>-V/B<sub>2</sub>O<sub>3</sub>, and CD<sub>s</sub>-VI/B<sub>2</sub>O<sub>3</sub> during continuous excitation with a UV lamp up to 60 min.

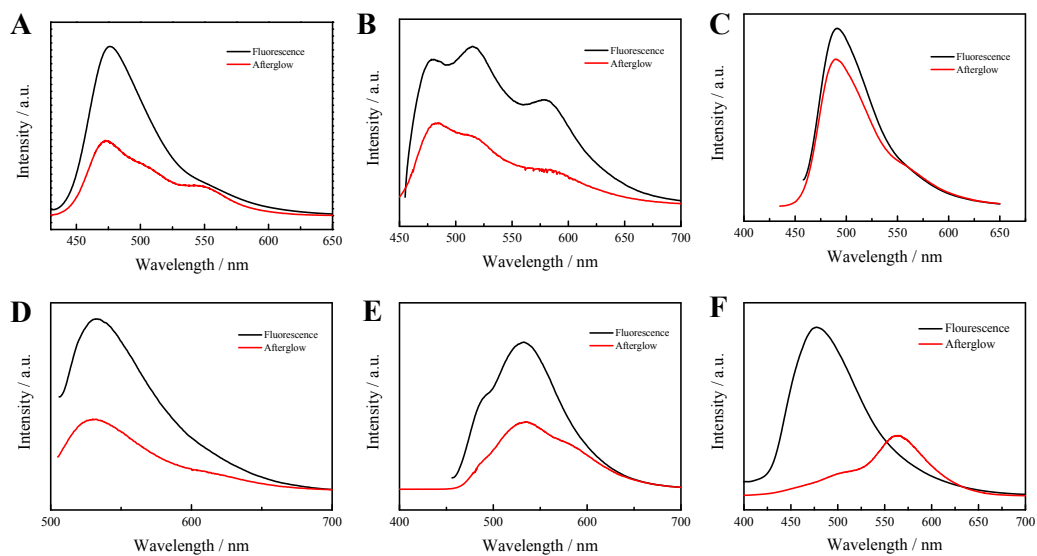


**Figure S13.** Fluorescence emission spectrum, and afterglow emission spectrum of (A) CD<sub>s</sub>-I/B<sub>2</sub>O<sub>3</sub>, (B) CD<sub>s</sub>-II/B<sub>2</sub>O<sub>3</sub>, (C) CD<sub>s</sub>-III/B<sub>2</sub>O<sub>3</sub>, (D) CD<sub>s</sub>-IV/B<sub>2</sub>O<sub>3</sub>, (E) CD<sub>s</sub>-V/B<sub>2</sub>O<sub>3</sub>, and (F) CD<sub>s</sub>-VI/B<sub>2</sub>O<sub>3</sub>.

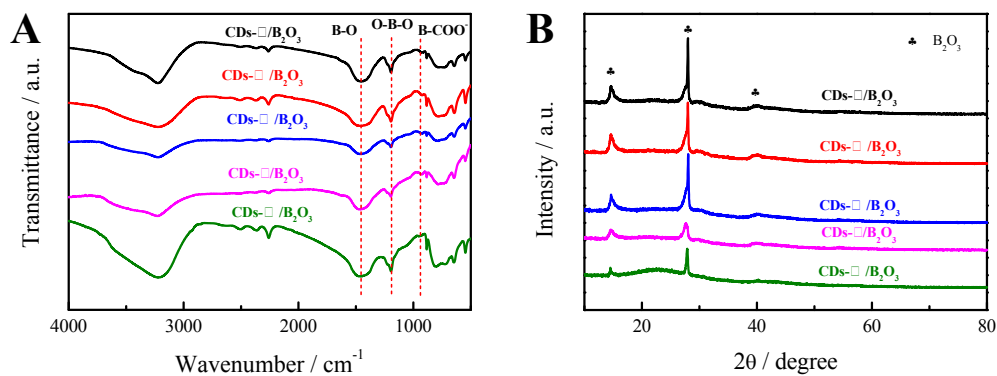


**Figure 14.** (A) FTIR spectra and (B) XRD patterns of CDs- II/B<sub>2</sub>O<sub>3</sub>, CDs-III/B<sub>2</sub>O<sub>3</sub>, CDs-IV/B<sub>2</sub>O<sub>3</sub>, CDs- V/B<sub>2</sub>O<sub>3</sub>, and CDs-VI/B<sub>2</sub>O<sub>3</sub>.

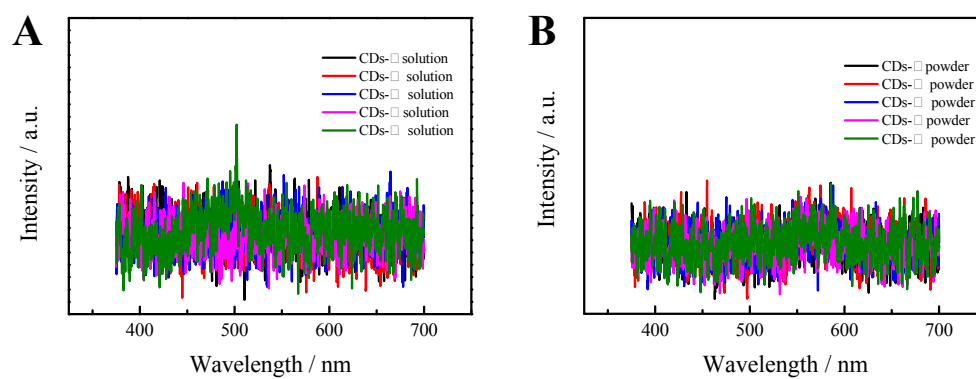


**Figure S15.** Afterglow spectra of (A) CDs solution(CDs- II, CDs-III, CDs-IV, CDs- V, and CDs-VI) and (B) CDs powder(CDs- II, CDs-III, CDs-IV, CDs- V, and CDs-VI).

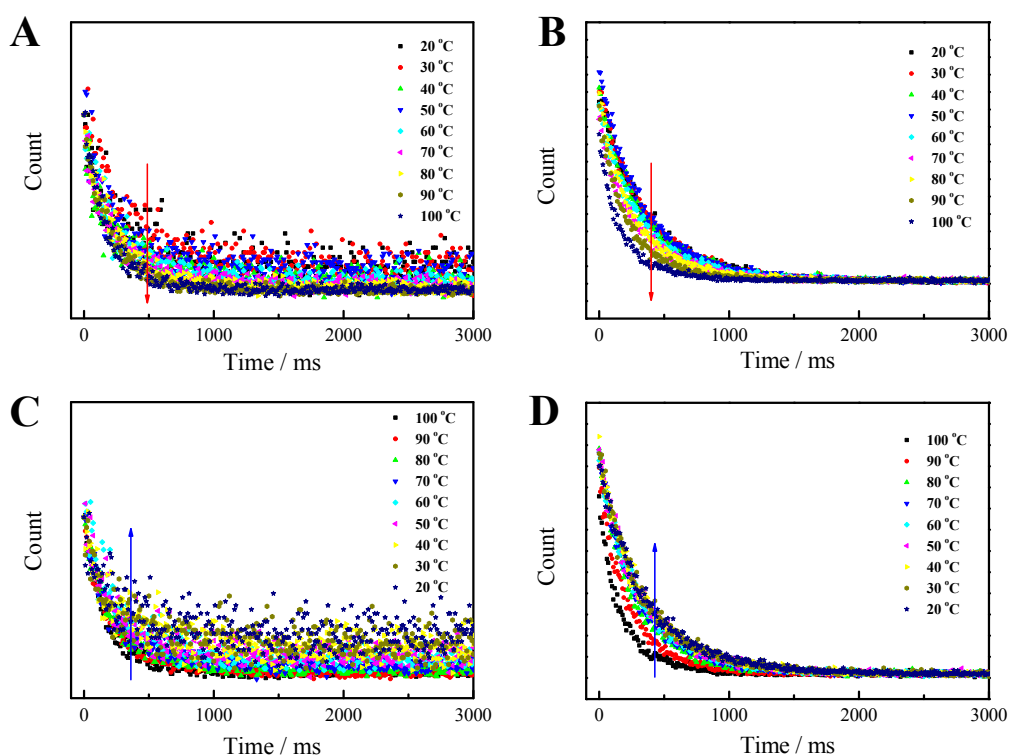


**Figure S16.** The afterglow decay curves of CDs-VI/B<sub>2</sub>O<sub>3</sub> composites at 477nm during (A)heating and (B)cooling process. The afterglow decay curves of CDs-VI/B<sub>2</sub>O<sub>3</sub> composites at 565nm during (C) heating and (D) cooling process.

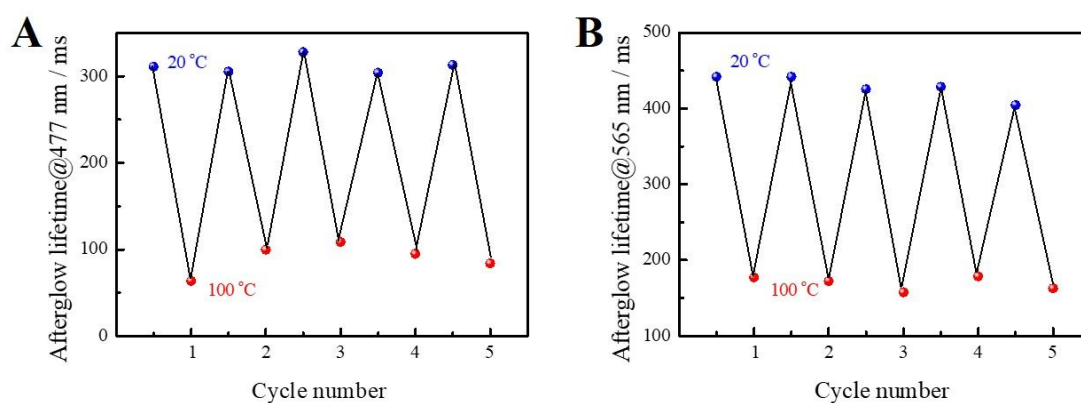


**Figure S17.** The lifetime cycle experiment of the temperature response over CDs-VI/B<sub>2</sub>O<sub>3</sub> composites at (A)477 nm and (B)565 nm. The afterglow lifetime of CDs-VI/B<sub>2</sub>O<sub>3</sub> composites was hardly changed subsequent to the five cycles of repetition, indicating that CDs-VI/B<sub>2</sub>O<sub>3</sub> composites have high stability and reversibility with temperature changes.

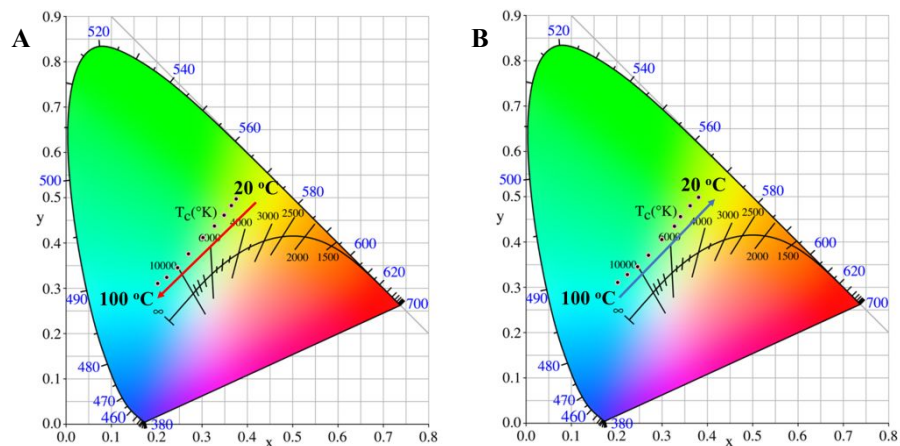


**Figure S18.** CIE coordinates of the afterglow emission of CDs-VI/B<sub>2</sub>O<sub>3</sub> composites during (A) heating and (B) cooling process.

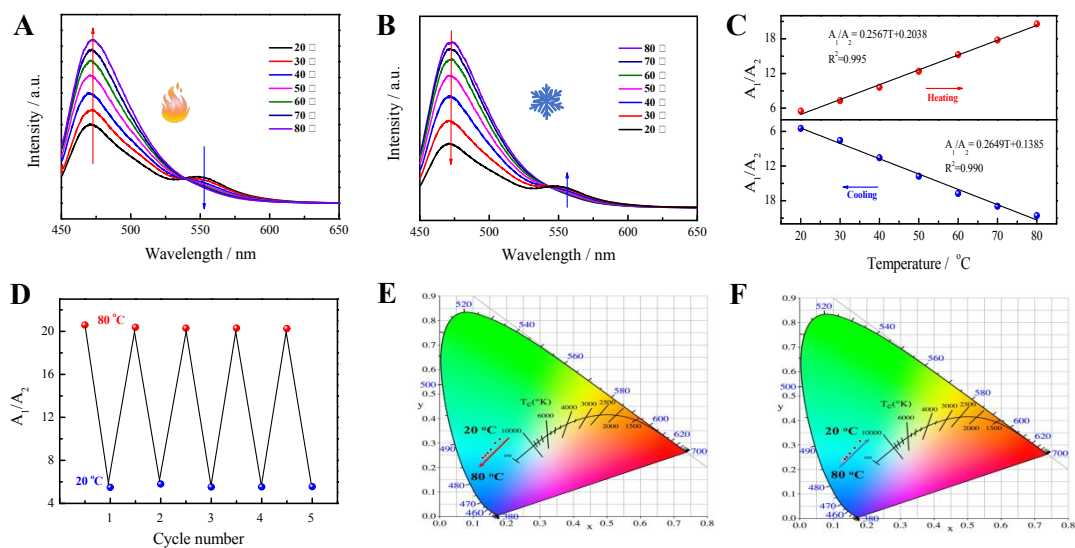


**Figure S19.** The afterglow emission spectra of CDs-I/B<sub>2</sub>O<sub>3</sub> composites during (A) heating and (B) cooling process with 440 nm excitation. (C) A<sub>1</sub>/A<sub>2</sub>-temperature plots of CDs-I/B<sub>2</sub>O<sub>3</sub> composites during heating and cooling process. (D) The cycle experiment of the temperature response over CDs-I/B<sub>2</sub>O<sub>3</sub> composites. CIE coordinates of the afterglow emission of CDs-I/B<sub>2</sub>O<sub>3</sub> composites during (E) heating and (F) cooling process.

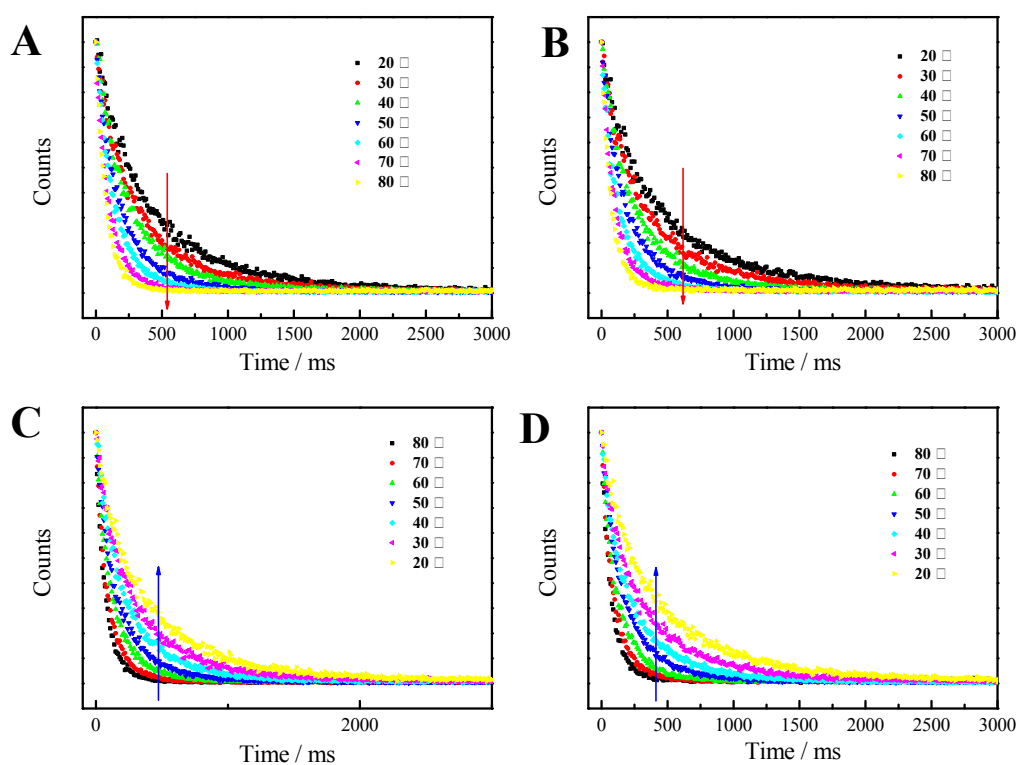


**Figure S20.** The afterglow decay curves of CDs-I/B<sub>2</sub>O<sub>3</sub> composites at 475nm during (A) heating and (B) cooling process. The afterglow decay curves of CDs-I/B<sub>2</sub>O<sub>3</sub> composites at 555nm during (C) heating and (D) cooling process.

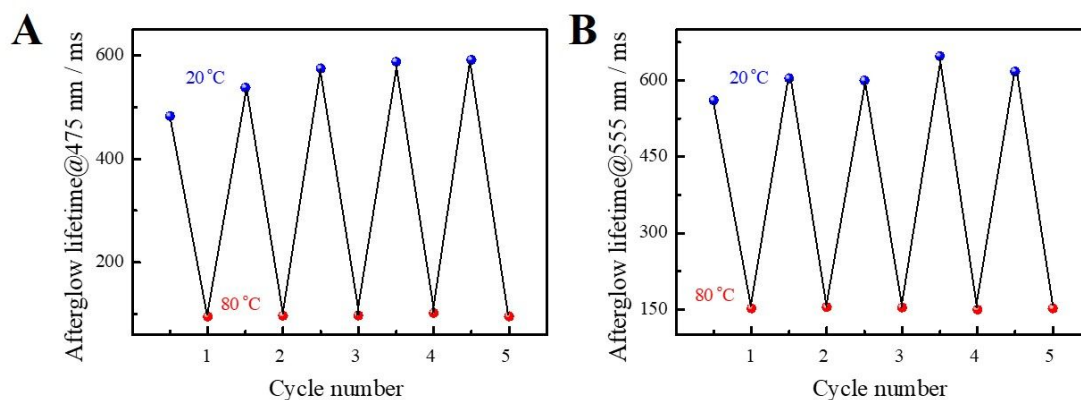


**Figure S21.** The lifetime cycle experiment of the temperature response over CDs-I/B<sub>2</sub>O<sub>3</sub> composites at (A)475 nm and (B)555 nm. The afterglow lifetime of CDs-I/B<sub>2</sub>O<sub>3</sub> composites was hardly changed subsequent to the five cycles of repetition, indicating that CDs-I/B<sub>2</sub>O<sub>3</sub> composites have high stability and reversibility with temperature changes.

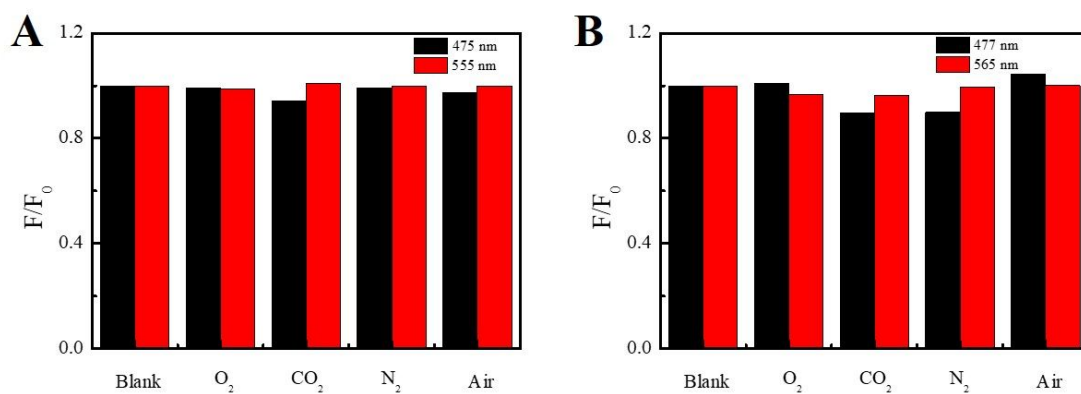


**Figure S22.** The afterglow intensity of (A)CDs-I/ $B_2O_3$  composites and (B)CDs-VI/ $B_2O_3$  composites after purging with oxygen, carbon dioxide, nitrogen, or air for 30 min.

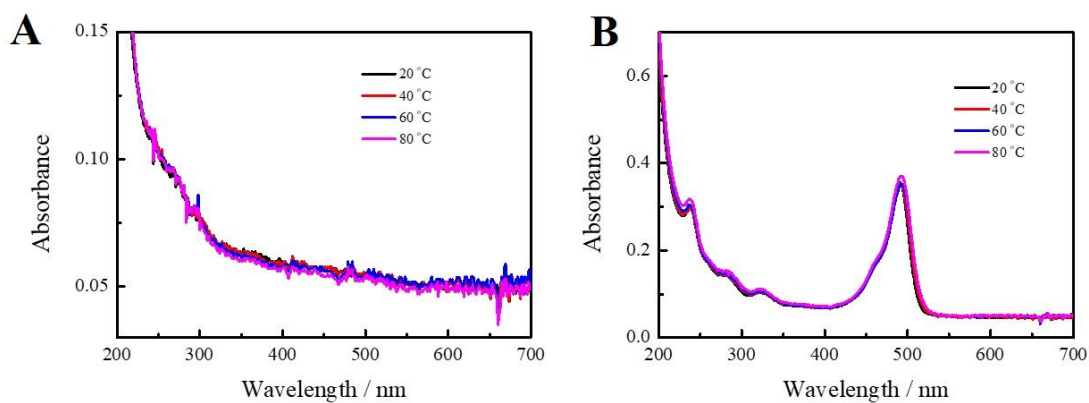


**Figure S23.** UV-vis spectra of (A) CDs-VI/ $B_2O_3$  composites and (B) CDs-I/ $B_2O_3$  composites with temperature increment

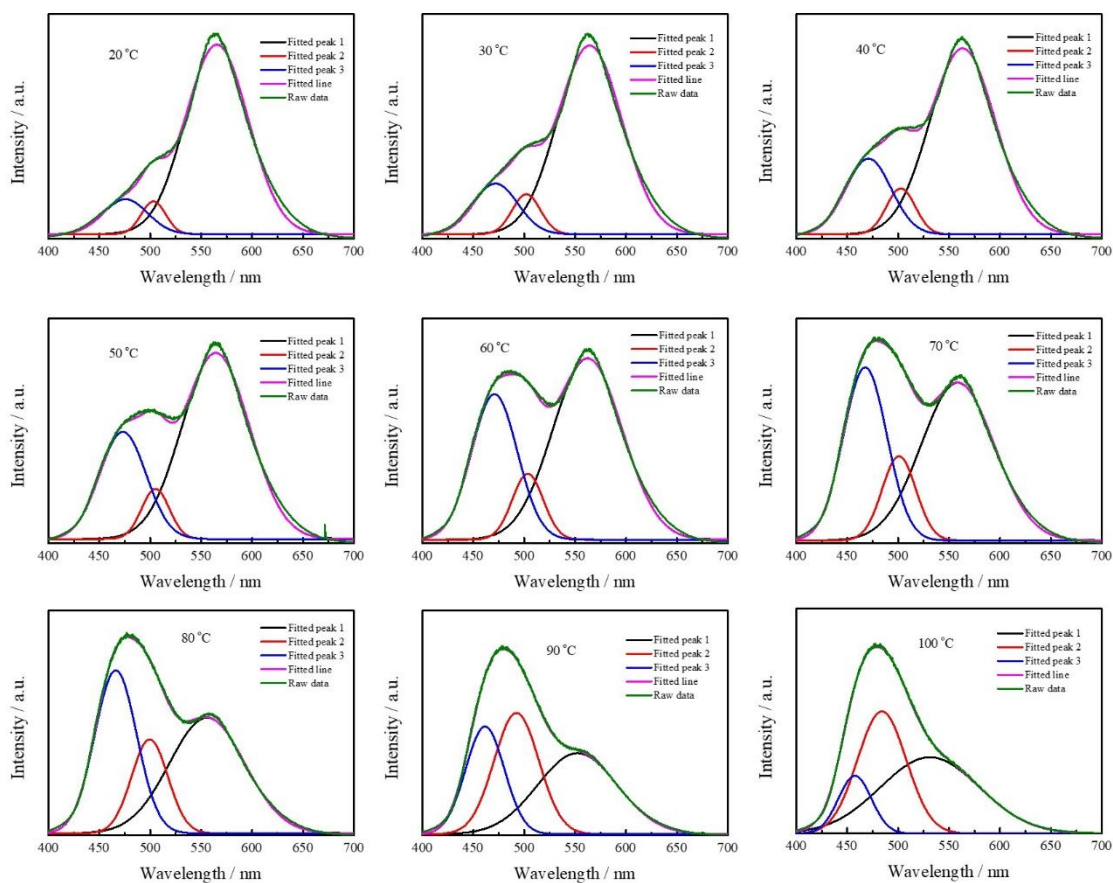


**Figure S24.** Deconvoluted afterglow spectra of CDs-VI/B<sub>2</sub>O<sub>3</sub> composites of with temperature increment.

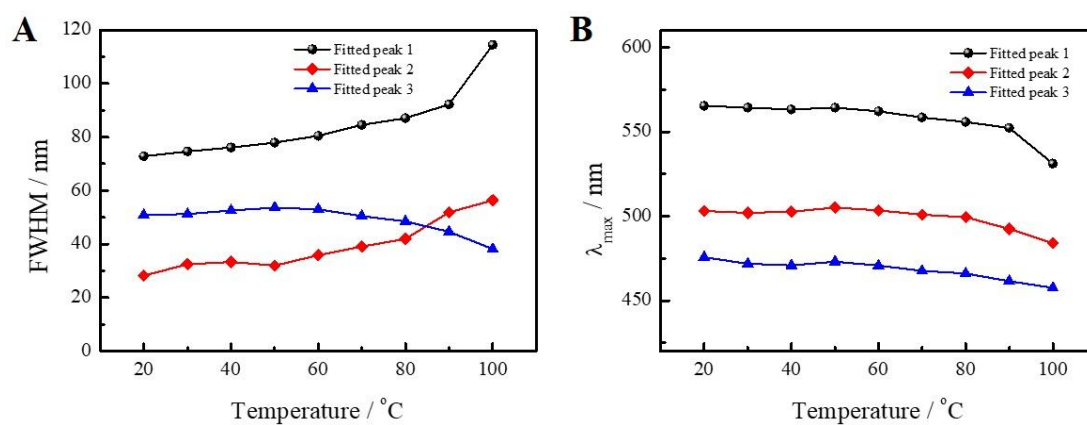


**Figure S25.** Corresponding temperature-dependent changes in the (A) PL fwhm and (B) PL peak maximum  $\lambda_{\text{max}}$  of CDs-VI/B<sub>2</sub>O<sub>3</sub> composites.

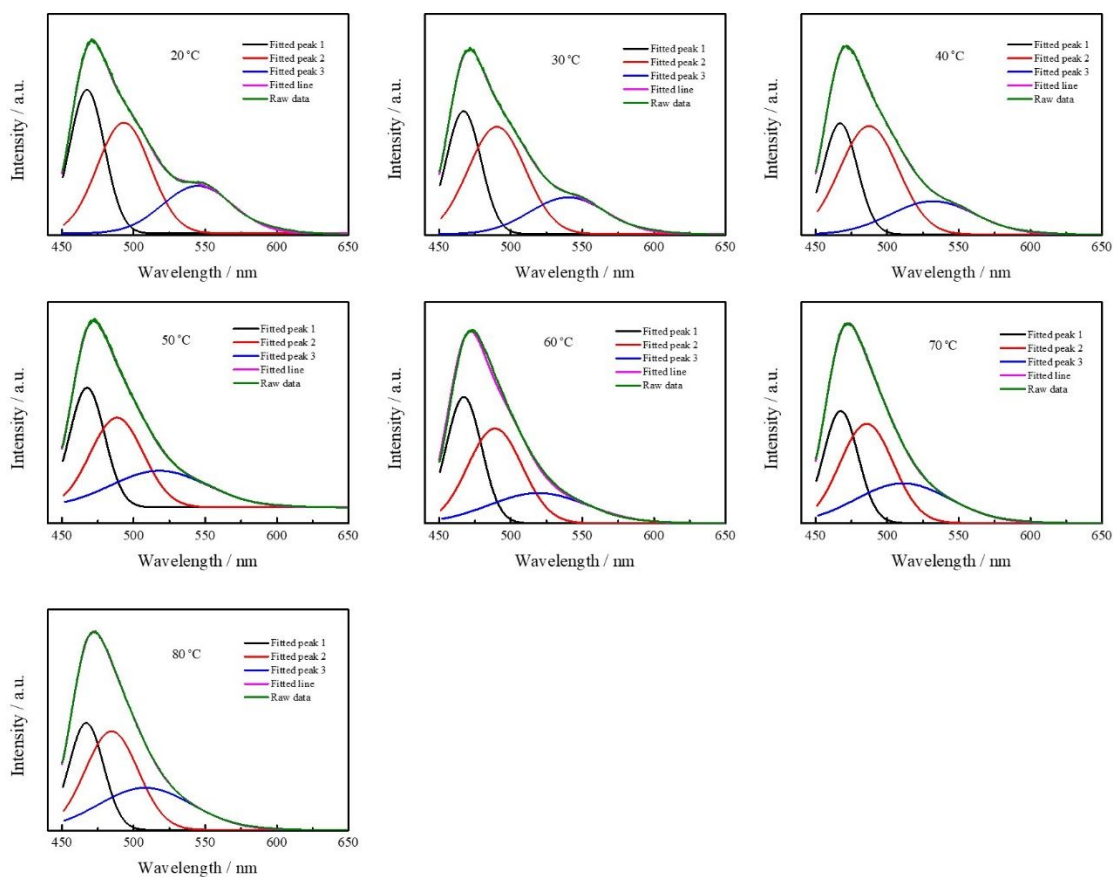


**Figure S26.** Deconvoluted afterglow spectra of CDs-I/B<sub>2</sub>O<sub>3</sub> composites of with temperature increment.

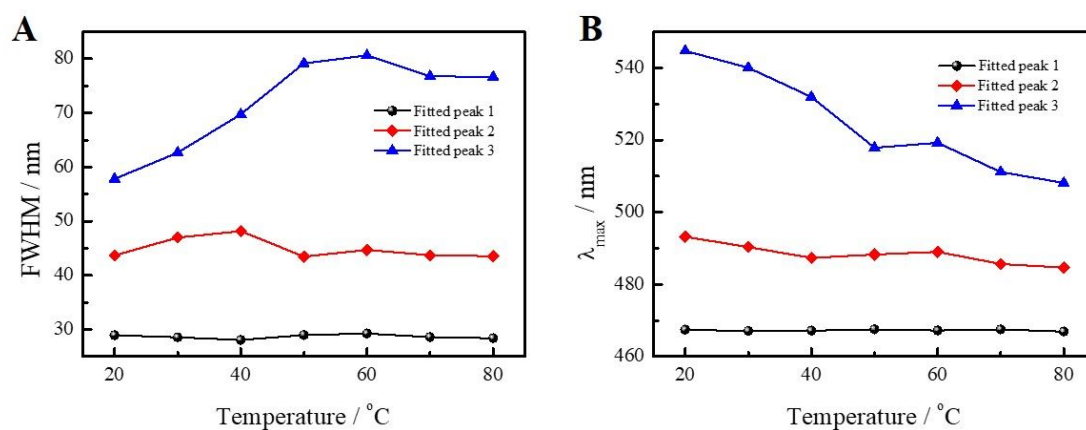


**Figure S27.** Corresponding temperature-dependent changes in the (A) PL fwhm and (B) PL peak maximum  $\lambda_{\text{max}}$  of CDs-I/B<sub>2</sub>O<sub>3</sub> composites.

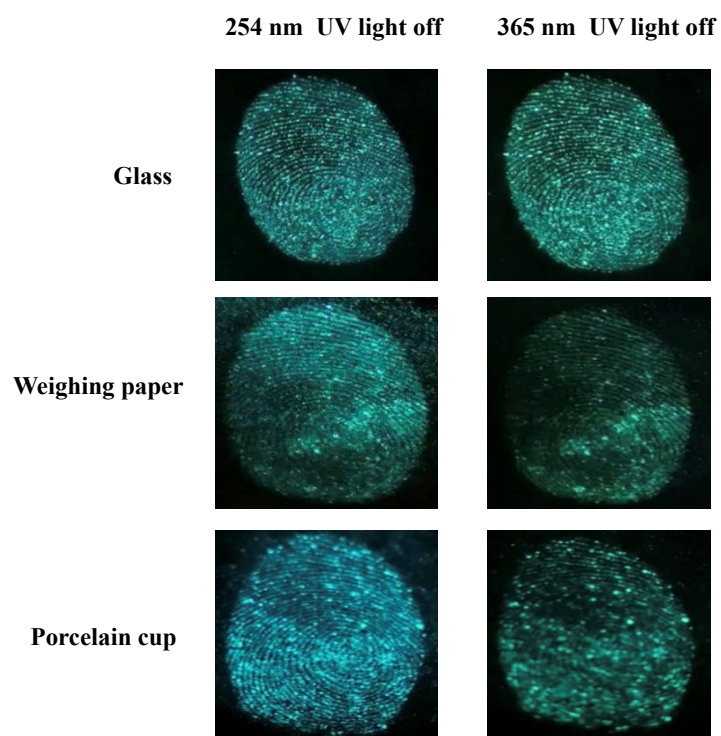


**Figure S28.** The images of LFPs on glass, weight paper and porcelain cup with CDs-I/B<sub>2</sub>O<sub>3</sub> after removing 254 nm and 365 nm light.

## Table

**Table S1** Comparison of quantum yield of the CDs-I solution with the reported methods

<b>raw material</b>	<b>synthetic method</b>	<b>quantum yield /%</b>	<b>refs.</b>
Citric acid and urea	Microwave assisted	11	4
Goat hooves	Microwave assisted	23.8	5
2-azidoimidazole and hydroxyl compounds	Microwave assisted	27.9	6
Graphite rod	Electrochemical exfoliation	16.5	7
Aloe	Hydrothermal	10.37	8
Smash	Hydrothermal	59	9
O-phenylenediamine and dopamine	Hydrothermal	33.96	10
O-phenylenediamine and HNO <sub>3</sub>	Hydrothermal	31.54	11
1,3,5-benzenetrithiol	Hydrothermal	31.82	12
rose bengal and branched polyethylenimine	Hydrothermal	90.49	13
Safranin T and NaOH	Hydrothermal	99.91	This work

**Table S2** Comparison the CDs-I/B<sub>2</sub>O<sub>3</sub> composites with the reported CDs-based afterglow materials.

afterglow materials	emission /nm	lifetime /ms	decay time by naked eyes /s	visible-light-excited	afterglow mode	quantum yield /%	refs.
TA-CDs	560	183.6	2.5	No	RTP	4.2	14
CDs	540	1510	12	Yes	RTP	11.5	15
AA-CDs	585	240.8	5	Yes	RTP	22.45	16
CDs/PVA nanofibers	456/569	1610	9	No	DF and RTP	22.57	17
G-CDs/B <sub>2</sub> O <sub>3</sub>	480/560	477.96	13	Yes	DF and RTP	38.06	1
m-CDs-PV A	485	456	-	No	RTP	-	18
a-CDs/BA	530	1600	8	No	RTP	8.7	19
MP-CDs	500-575	880	8	No	RTP	2.4	20
CQDs/PU	500	8.7	-	No	RTP	-	21
HN-CDs	490	1060	-	No	RTP	7	22
CDs@SBT-2	440	153	-	No	DF	29.45	23
Zn-CDs-LD Hs	490	719.9	5	No	RTP	9.58	24
CDs-1	518	106	3	No	RTP	5.3	25
CDs@MnA PO-CJ50	620	10.94	0.119	No	RTP	9.6	26
CDs/PVA	510	271.2	-	No	RTP	-	27
CDs@Zn-C HA	500	22.32	-	No	RTP	14.1	28
CDs@Mn-L EV	620	18.14	-	No	RTP	5.7	28
CDs-I/B <sub>2</sub> O <sub>3</sub>	475/555	423.5/ 445.9	8	Yes	DF and RTP	17.61	This work

## Reference

- (1) Xu, Z.; Sun, X.; Ma, P.; Chen, Y.; Pan, W.; Wang, J. A visible-light-excited afterglow achieved by carbon dots from rhodamine b fixed in boron oxide. *Journal of Materials Chemistry C* **2020**, *8* (13), 4557-4563. DOI: 10.1039/C9TC05992J.
- (2) Zhou, W.; Zhuang, J. L.; Li, W.; Hu, C. F.; Lei, B. F.; Liu, Y. L. Towards efficient dual-emissive carbon dots through sulfur and nitrogen co-doped. *Journal of Materials Chemistry C* **2018**, *6* (12), 3104-3104. DOI: 10.1039/C7TC01819C.
- (3) He, W.; Weng, W.; Sun, X.; Pan, Y.; Chen, X.; Liu, B.; Shen, J. Multifunctional carbon dots with solid-liquid state orange light emission for vitamin B12 sensing, cellular imaging, and red/white light-emitting diodes. *Acs Appl Nano Mater* **2020**, *3* (8), 7420-7427. DOI: 10.1021/acsanm.0c01003
- (4) Li, D.; Liang, C.; Ushakova, E. V.; Sun, M.; Huang, X.; Zhang, X.; Jing, P.; Yoo, S. J.; Kim, J. G.; Liu, E.; Zhang, W.; Jing, L.; Xing, G.; Zheng, W.; Tang, Z.; Qu, S.; Rogach, A. L. Thermally activated upconversion near-infrared photoluminescence from carbon dots synthesized via microwave assisted exfoliation. *Small* **2019**, *15* (50), e1905050. DOI: 10.1002/smll.201970288.
- (5) Raji, K.; Vadivel, R.; Thiyagarajan, S. K.; Ramamurthy, P. Environmentally benign, facile and selective recovery of gold from aqueous media: synergic role of carbon dots as green reductant and sensor towards Au<sup>3+</sup> ions. *Rsc Adv* **2019**, *9* (68), 39689-39698. DOI: 10.1039/C9RA08050C
- (6) Feng, J.; Zhao, X.; Bian, W.; Tang, X. Microwave-assisted synthesis of nitrogen-rich carbon dots as effective fluorescent probes for sensitive detection of Ag<sup>+</sup>. *Mat Chem Front* **2019**, *3* (12), 2751-2758. DOI: 10.1039/C9QM00624A.
- (7) Ming, H.; Ma, Z.; Liu, Y.; Pan, K.; Yu, H.; Wang, F.; Kang, Z. Large scale electrochemical synthesis of high quality carbon nanodots and their photocatalytic property. *Dalton Trans* **2012**, *41* (31), 9526-9531. DOI: 10.1039/c2dt30985h.
- (8) Xu, H.; Yang, X.; Li, G.; Zhao, C.; Liao, X. Green synthesis of fluorescent carbon dots for selective detection of tartrazine in food samples. *J Agric Food Chem* **2015**, *63* (30), 6707-6714. DOI: 10.1021/acs.jafc.5b02319.
- (9) Liu, J.; Geng, Y.; Li, D.; Yao, H.; Huo, Z.; Li, Y.; Zhang, K.; Zhu, S.; Wei, H.; Xu, W.; Jiang, J.; Yang, B. Deep red emissive carbonized polymer dots with unprecedented narrow full width at half maximum. *Adv Mater* **2020**, *32* (17), e1906641. DOI: 10.1002/adma.201906641.
- (10) Wang, B.; Li, J.; Tang, Z.; Yang, B.; Lu, S. Near-infrared emissive carbon dots with 33.96% emission in aqueous solution for cellular sensing and light-emitting diodes. *Science Bulletin* **2019**, *64* (17), 1285-1292. DOI: 10.1016/j.scib.2019.07.021
- (11) Liu, J.; Li, D.; Zhang, K.; Yang, M.; Sun, H.; Yang, B. One-step hydrothermal synthesis of nitrogen-doped conjugated carbonized polymer dots with 31% efficient red emission for in vivo imaging. *Small* **2018**, *14* (15), e1703919. DOI: 10.1002/smll.201703919.

- (12) Wang, Q.; Zhang, S.; Wang, B.; Yang, X.; Zou, B.; Yang, B.; Lu, S. Pressure-triggered aggregation-induced emission enhancement in red emissive amorphous carbon dots. *Nanoscale Horizons* **2019**, *4* (5), 1227-1231. DOI: 10.1039/C9NH00287A.
- (13) Tong, L.; Wang, X.; Chen, Z.; Liang, Y.; Yang, Y.; Gao, W.; Liu, Z.; Tang, B. One-step fabrication of functional carbon dots with 90% fluorescence quantum yield for long-term lysosome imaging. *Anal Chem* **2020**, *92* (9), 6430-6436. DOI: 10.1021/acs.analchem.9b05553
- (14) Jiang, K.; Gao, X.; Feng, X.; Wang, Y.; Li, Z.; Lin, H. Carbon dots with dual-emissive, robust, and aggregation-induced room-temperature phosphorescence characteristics. *Angew Chem Int Ed Engl* **2020**, *59* (3), 1263-1269. DOI: 10.1002/anie.201911342.
- (15) Gao, Y.; Zhang, H.; Shuang, S.; Dong, C. Visible-light-excited ultralong-Lifetime room temperature phosphorescence based on nitrogen-doped carbon dots for double anticounterfeiting. *Advanced Optical Materials* **2020**, *8* (7), 1901557. DOI: 10.1002/adom.201901557.
- (16) Hu, S.; Jiang, K.; Wang, Y.; Wang, S.; Li, Z.; Lin, H. Visible-light-excited room temperature phosphorescent carbon dots. *Nanomaterials (Basel)* **2020**, *10* (3), 464. DOI: 10.3390/nano10030464.
- (17) He, J.; He, Y.; Chen, Y.; Zhang, X.; Hu, C.; Zhuang, J.; Lei, B.; Liu, Y. Construction and multifunctional applications of carbon dots/pva nanofibers with phosphorescence and thermally activated delayed fluorescence. *Chem Eng J* **2018**, *347*, 505-513. DOI: 10.1016/j.cej.2018.04.110.
- (18) Jiang, K.; Zhang, L.; Lu, J.; Xu, C.; Cai, C.; Lin, H. Triple-mode emission of carbon dots: applications for advanced anti-counterfeiting. *Angew Chem Int Ed Engl* **2016**, *55* (25), 7231-7235. DOI: 10.1002/anie.201602445.
- (19) Li, W.; Zhou, W.; Zhou, Z.; Zhang, H.; Zhang, X.; Zhuang, J.; Liu, Y.; Lei, B.; Hu, C. A universal strategy for activating the multicolor room-temperature afterglow of carbon dots in a boric acid matrix. *Angew Chem Int Ed Engl* **2019**, *58* (22), 7278-7283. DOI: 10.1002/anie.201814629.
- (20) Jiang, K.; Hu, S.; Wang, Y.; Li, Z.; Lin, H. Photo-stimulated polychromatic room temperature phosphorescence of carbon dots. *Small* **2020**, *16* (31), e2001909. DOI: 10.1002/smll.202001909.
- (21) Tan, J.; Zou, R.; Zhang, J.; Li, W.; Zhang, L.; Yue, D. Large-scale synthesis of n-doped carbon quantum dots and their phosphorescence properties in a polyurethane matrix. *Nanoscale* **2016**, *8* (8), 4742-4747. DOI: 10.1039/c5nr08516k.
- (22) Li, Q.; Zhou, M.; Yang, Q.; Wu, Q.; Shi, J.; Gong, A.; Yang, M. Efficient room-temperature phosphorescence from nitrogen-doped carbon dots in composite matrices. *Chem Mater* **2016**, *28* (22), 8221-8227. DOI: 10.1021/acs.chemmater.6b03049.
- (23) Zhang, H.; Liu, J.; Wang, B.; Liu, K.; Chen, G.; Yu, X.; Li, J.; Yu, J. Zeolite-confined carbon dots: tuning thermally activated delayed fluorescence emission via energy transfer. *Mat Chem Front* **2020**, *4* (5), 1404-1410. DOI: 10.1039/C9QM00549H.
- (24) Kong, X.; Wang, X.; Cheng, H.; Zhao, Y.; Shi, W. Activating room temperature

phosphorescence by organic materials using synergistic effects. *Journal of Materials Chemistry C* **2019**, *7* (2), 230-236. **DOI:** 10.1039/C8TC04482A.

(25) Zhao, F.; Zhang, T.; Liu, Q.; Lü, C. Aphen-derived N-doped white-emitting carbon dots with room temperature phosphorescence for versatile applications. *Sensors and Actuators B: Chemical* **2020**, *304*, 127344. **DOI:** 10.1016/j.snb.2019.127344.

(26) Wang, B.; Yu, Y.; Zhang, H.; Xuan, Y.; Chen, G.; Ma, W.; Li, J.; Yu, J. Carbon dots in a matrix: energy-transfer-enhanced room-temperature red phosphorescence. *Angew Chem Int Ed Engl* **2019**, *58* (51), 18443-18448. **DOI:** 10.1002/anie.201911035.

(27) Wu, X.; Ma, C.; Liu, J.; Liu, Y.; Luo, S.; Xu, M.; Wu, P.; Li, W.; Liu, S. In situ green synthesis of nitrogen-doped carbon-dot-based room-temperature phosphorescent materials for visual iron ion detection. *Acs Sustain Chem Eng* **2019**, *7* (23), 18801-18809. **DOI:** 10.1021/acssuschemeng.9b03281.

(28) Wang, B.; Mu, Y.; Zhang, H.; Shi, H.; Chen, G.; Yu, Y.; Yang, Z.; Li, J.; Yu, J. Red room-temperature phosphorescence of CDs@Zeolite composites triggered by heteroatoms in zeolite frameworks. *ACS Cent Sci* **2019**, *5* (2), 349-356. **DOI:** 10.1021/acscentsci.8b00844.